1439

LA-9912-MS

KERRISK

Los Alamos National Laboratory is operated by the University of California for the United States Department of Energy under contract W-7405-ENG-36

Reaction-Path Calculations of Groundwater Chemistry and Mineral Formation at Rainier Mesa, Nevada

Los Alamos National Laboratory
Los Alamos, New Mexico 87545

LA-9912-MS

UC-70
Issued: December 1983

Reaction-Path Calculations of Groundwater Chemistry and Mineral Formation at Rainier Mesa, Nevada

Jerry F. Kerrisk

Los Alamos National Laboratory
Los Alamos, New Mexico 87545

REACTION-PATH CALCULATIONS OF GROUNDWATER CHEMISTRY AND MINERAL FORMATION AT RAINIER MESA, NEVADA

By

Jerry F. Kerrisk

ABSTRACT

Reaction-path calculations of groundwater chemistry and mineral formation at Rainier Mesa, Nevada, have been done using a model of volcanic-glass dissolution by water that is initially saturated with CO_2. In the reaction-path calculation, rate processes control the availability of species through dissolution of volcanic glass, and equilibrium processes distribute the species between the aqueous phase and mineral phases in equilibrium at each step in the reaction path. The EQ3/6 chemical-equilibrium programs were used for the calculation. Formation constants were estimated for three zeolites (clinoptilolite, mordenite, and heulandite), so they could be considered as possible mineral precipitates. The first stage of mineral evolution, from volcanic glass to a cristobalite, smectite clay, and zeolite mixture, was modeled quite well. Predicted aqueous-phase compositions and precipitates agree with observations at Rainier Mesa and other Nevada Test Site areas. Further mineral evolution, to quartz, clay, analcime, and albite mixtures, was also modeled. Decreasing aqueous silica activity from the first stage, where cristobalite precipitates, to later stages, where quartz is present, was the controlling variable in the mineral evolution.

I. INTRODUCTION

Yucca Mountain, which is on and adjacent to the Nevada Test Site (NTS) in south-central Nevada, is being studied as a potential site for storage of high-level radioactive waste. These studies are part of the Nevada Nuclear Waste

they are useful because there are large areas at NTS where minerals from the various stages predominate.

This paper describes reaction-path calculations of groundwater chemistry and mineral formation that are based on the model proposed by Claassen and White (1978). The reaction-path calculation models an essentially irreversible process (the dissolution of volcanic glass and precipitation of other minerals) as a sequence of partial equilibrium states (Helgeson 1968; Helgeson et al. 1969; Wolery 1979). The initial state of the system is water saturated with CO_2 at the temperature of interest. At each subsequent step in the sequence, additional glass dissolution products are added to the system in amounts proportional to their relative dissolution rates. An equilibrium calculation is performed to distribute the various species among the aqueous and mineral phases that are in equilibrium under the conditions of that step. The result of the calculation is a sequence of aqueous-phase compositions and mineral assemblages that would exist if the overall process were controlled by glass dissolution and all other processes were in equilibrium. The reaction-path calculation does not describe the overall irreversible process as a function of time, but in terms of a variable called the reaction progress. For these calculations, reaction progress is proportional to the amount of dissolution of volcanic glass. A direct relation between predicted system compositions and time cannot be made without additional rate data. Although actual dissolution rates were measured for the Rainier Mesa glass, the relation between time and the predicted compositions was not established here because it would have required an assumption about glass surface area available for dissolution (White et al. 1980; Claassen and White 1978).

The calculations presented here represent a very simplified model of a complex geologic system. Only the major chemical components are included in the model, and only equilibrium processes are considered at each step in the reaction path. However, the calculations do represent a step in the direction of a more quantitative treatment of the relation between groundwater and minerals at NTS. In this respect, they provide a test of whether equilibrium processes are important in controlling the mineral assemblage. The model also provides a tool for examining effects of changes in various parameters (temperature, for example) on equilibrium groundwater chemistry and mineral assemblages.

White et al. (1980) measured dissolution rates of SiO_2(aq), Na^+, K^+, Ca^{2+}, and Mg^{2+} at 25°C from Rainier Mesa volcanic glass as a function of pH. Their results showed an initial rapid dissolution rate followed by a steady-state (parabolic) rate over longer times. Following the assumption of Claassen and White (1978), steady-state rates were used here. Because the reaction-progress variable is not directly related to time, only relative dissolution rates were needed for these calculations. The dissolution rates were normalized so that the SiO_2(aq) dissolution rate was 1. Under these conditions, the reaction-progress variable is equal to the moles of SiO_2(aq) dissolved from the glass. Dissolution rates for SiO_2(aq) and K^+ were found to be essentially independent of pH, whereas rates for Na^+, Ca^{2+}, and Mg^{2+} decreased with increasing pH (White et al. 1980). Figure 1 shows a plot of the dissolution rates of these five species used for the calculations.

To precipitate most of the minerals observed at Rainier Mesa, it was necessary to also have aluminum and iron in the calculation. Dissolution rates for these species were not measured. It was assumed that the Al^{3+} dissolution rate [relative to SiO_2(aq)] was constant and was the same as the aluminum/silicon ratio of the Rainier Mesa volcanic glass (White et al. 1980). The rate used was 0.22 moles of Al^{3+} per mole of SiO_2(aq). Iron was not determined in this glass; a constant dissolution rate for Fe^{3+} was assumed, based on compositions of similar volcanic glasses found near Rainier Mesa (Essington and Sharp 1968). The rate used was 0.02 moles of Fe^{3+} per mole of SiO_2(aq). Ferric iron was assumed to be the dissolution product because the initial aqueous phase was taken as oxidizing, being in contact with O_2(g) at 0.2 atm fugacity (Noble 1967). Figure 1 also shows the nominal dissolution rates of Al^{3+} and Fe^{3+} plotted with the other dissolution-rate data. Because Al^{3+} and Fe^{3+} dissolution rates were assumed rather than measured, some reaction-path calculations were done with higher and lower dissolution rates for these species to assess the effect of different rates on the results.

As proposed by Claassen and White (1978), the dissolution process is actually an ion-exchange reaction in which H^+ from the aqueous phase is exchanged for the cations from the volcanic glass to maintain electrical neutrality. This reaction was modeled by assuming that OH^- is one of the dissolution products and by calculating the OH^- dissolution rate to maintain electrical neutrality (see Fig. 1). The technique of adding aqueous species to the aqueous phase to simulate glass dissolution ignores the detailed

was followed with quartz and chalcedony for many of the calculations to increase the $SiO_2(aq)$ activity and with other minerals to change other aqueous-phase activities. Although the method of suppressing precipitation of particular minerals to simulate kinetic constraints on precipitation is a rough approximation to reality, it does serve to bracket the expected conditions of the system and thus can give useful information.

The reaction-path calculations were done with the EQ3/6 chemical-equilibrium computer programs, version 3175B, which were released in August 1982 (Wolery 1979; Wolery 1980). The EQ3 program, which performs a speciation calculation at the start of a run, was used without modification. The EQ6 program, which performs the reaction-path calculation, was modified to allow the dissolution rates of the various species from the volcanic glass to vary with pH of the aqueous phase. The thermodynamic data base employed for these calculations contained data for 223 minerals, 293 aqueous complexes, and 14 solid solutions. These totals include the zeolite data discussed in the following section. Most of the mineral data and much of the aqueous-complex data are from compilations by Helgeson et al. (1970) and Helgeson et al. (1978). Most of the solid solutions are treated as ideal solutions; this is certainly an approximation, but it is generally necessary because of a lack of data. The Appendix contains a list of compositions of the minerals and solid-solution end members referred to in this paper, as defined in the EQ3/6 data base. Calculations were done at temperatures from 25 to 175°C because temperature was considered one of the important parameters in this analysis. Thermodynamic data are available from 0 to 300°C for most species in the EQ3/6 data base; however, the volcanic-glass dissolution rates measured at 25°C were used in all calculations. Although absolute dissolution rates should increase rapidly with increasing temperature, the relative rates used in the reaction-path calculation would be affected much less by temperature. Calculations and thermodynamic data are for a total pressure of 1 atm up to 100°C and for the saturation pressure of water at higher temperatures.

III. ZEOLITE THERMODYNAMIC DATA ESTIMATES

Zeolites, with silica and clays, form much of the alteration products observed at Rainier Mesa and other NTS locations. Thus, to model mineral formation in these areas, these minerals should be included in the thermodynamic data base. Of the three zeolites in the normal EQ3/6 data base

TABLE I

ZEOLITE FORMULAE

Clinoptilolite	Mordenite
$Na_2[Al_2Si_{10}O_{24}]\cdot 8H_2O$	$Na[AlSi_5O_{12}]\cdot 3H_2O$
$K_2[Al_2Si_{10}O_{24}]\cdot 8H_2$	$K[AlSi_5O_{12}]\cdot 3H_2O$
$Ca[Al_2Si_{10}O_{24}]\cdot 8H_2O$	Heulandite
$Mg[Al_2Si_{10}O_{24}]\cdot 8H_2O$	$Ca[Al_2Si_7O_{18}]\cdot 6H_2O$

only be used at 25°C because they require special sets of thermodynamic data or correction constants that have been determined at that temperature only. Chen's method uses a sequence of reactions forming the mineral of interest from simpler compounds to estimate ΔG_f^o for the mineral. As long as ΔG_f^o data are available for the simpler compounds as a function of temperature, Chen's method can be used at any temperature. Because of its flexibility, the method proposed by Chen was used for the zeolite estimates reported here.

A group of minerals for which thermodynamic data are available in the range 0 to 300°C, and which can be used as the simpler compounds in Chen's method for these zeolites, is available in the EQ3/6 data base. These minerals, supplemented by data for Na_2O, K_2O, CaO, and MgO from the SUPCRT compilation (Helgeson et al. 1978), were used (see list in Table II). An advantage of using data from the EQ3/6 data base for estimations is that it provides zeolite data that are consistent with the other thermodynamic data employed in the reaction-path calculations. Values of $\log_{10} K_f$ for formation reactions from the EQ3/6 basis species were available as a function of temperature for all the species listed in Table II. Rather than converting these data to ΔG_f^o data, doing the estimation, and converting the results back to $\log_{10} K_f$ data, the equivalent procedure of estimating $\log_{10} K_f$ data for the zeolites directly from $\log_{10} K_f$ data for the simpler compounds was used. In other respects, Chen's method was used as originally proposed. Estimates were made at 0, 25, 60, 100, 150, 200, 250, and 300°C. Figures 2 and 3 show plots of $\log_{10} K_f$ as a function of temperature for the seven pure-component zeolites listed in Table I.

It is difficult to judge the accuracy of these estimates. As a test of the method and data, estimates were also made of $\log_{10} K_f$ for $CaAl_2Si_4O_{12}\cdot 2H_2O$

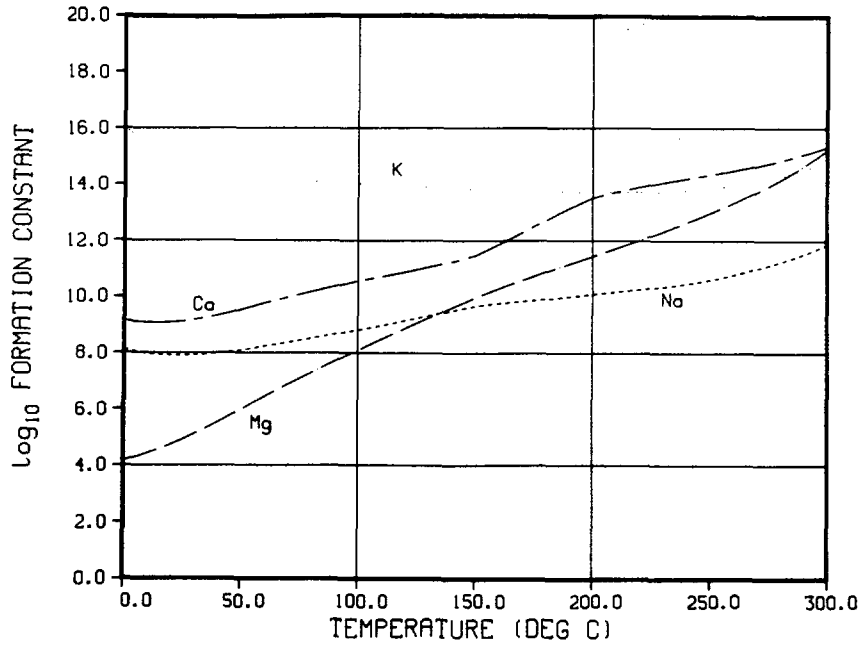

Fig. 2. Clinoptilolite formation constants.

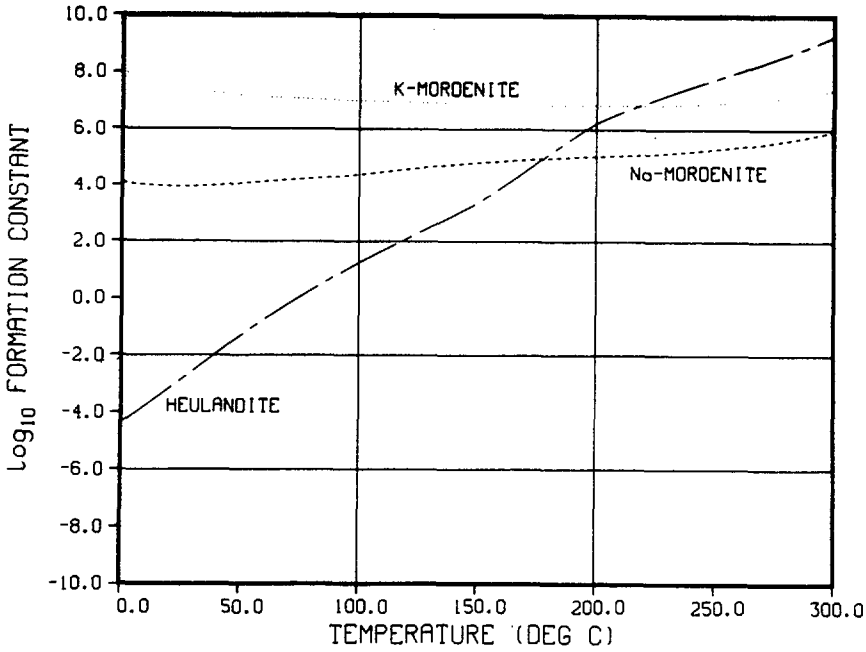

Fig. 3. Mordenite and heulandite formation constants.

they cool to 25°C. The change in pH of these solutions with temperature is a second-order effect and will be neglected in discussing the results of the calculations.

The general trend of the results is the same for all cases. In early stages of the reaction path (reaction progress $<\sim10^{-4}$), aqueous-phase composition is controlled by the dissolution process; few or no precipitates have formed. Solution pH starts at 4.5, the pH assumed for the initial glass-free carbonate solution, and it increases with increasing reaction progress. In intermediate stages ($\sim10^{-4}$ < reaction progress $<\sim10^{-1}$), various minerals precipitate and begin to control the aqueous-phase composition. In the latter stages of the reaction path (reaction progress $>\sim10^{-1}$), a stable mineral assemblage has formed that controls the aqueous-phase composition. Solid-solution compositions in the mineral assemblage and the aqueous-phase composition change slowly with increasing reaction progress, approaching a steady-state condition, where the aqueous-phase composition is constant and the dissolution rate of each species equals the rate of accumulation of that species in the mineral assemblage. All calculations were run to a reaction progress of at least 0.2. By this time, a stable mineral assemblage had usually formed, although compositions of solid solutions, and thus the aqueous phase, were still changing slowly with increasing reaction progress. Calculations were run to a reaction progress of 0.4 to 0.8 in a few cases where obvious changes were still occurring at 0.2 and in a few other cases to test the stability of the mineral assemblage.

A. No Precipitates Suppressed

The first calculations done suppressed none of the minerals in the data base. Figure 4 shows a plot of aqueous-phase pH as a function of reaction progress for calculations at 25, 75, and 125°C. The pH starts at 4.5 and rises to 8 to 10, where it is controlled by the mineral assemblage. The pH of Rainier Mesa water is generally in the range of 7 to 8. Thus, the predicted mineral assemblage in this case results in a solution pH that is higher than observed, although as temperature increases, solution pH is decreasing toward the observed range. At pH 7, the total dissolved silica content of the aqueous phase is 0.1 mmolal at 25°C, 0.5 mmolal at 75°C, and 1.3 mmolal at 125°C; at 25 and 75°C, this is below the 0.7 to 1.3 mmolal range observed for Rainier Mesa water. Figure 5 shows a plot of total sodium, potassium, calcium, and magnesium content of the aqueous phase as a function of reaction progress at

75°C. The vertical lines at the left side of the figure represent ranges observed for these species at Rainier Mesa (White et al. 1980).

Another way to compare the alkali metal and alkaline earth compositions of the aqueous phase with observations is with a ternary diagram. Figure 6 shows the relative Na-K-Ca compositions at 25, 75, and 125°C on a ternary diagram. The line for each temperature represents the entire reaction path from the start (40% sodium, 57% calcium, and 3% potassium) to a reaction progress of 0.2 or greater (essentially all sodium). The shaded area represents the range of relative composition observed at Rainier Mesa (White et al. 1980). At the start of the reaction-path calculation, the relative compositions at all temperatures are essentially the same, being dominated by the dissolution rates of these species from the glass. As reaction progress increases, the relative sodium content steadily increases, the relative calcium content steadily decreases, whereas the relative potassium content remains in the 0 to 15% range. The reaction paths at 25 and 75°C remain on the low-potassium side of the observed range, but at 125°C, the reaction path agrees with observations. A similar plot for relative Na-K-Mg compositions shows that the 25°C reaction path also remains on the low-potassium side of the observed range, but the higher temperature reaction paths agree well with observations. The trend of both relative-composition plots with increasing reaction progress, that is, toward the sodium apex, is the same as the trend of observations on interstitial water with increasing depth at Rainier Mesa (White et al. 1980). Thus, the shaded areas near the sodium apex represent the deepest interstitial water compositions, whereas the shaded regions farthest from the sodium apex represent the shallowest compositions.

Figure 7 shows a plot of the total quantities of the various minerals precipitated (moles per kilogram of water in the aqueous phase) at 75°C as a function of reaction progress. In addition to those present in the final mineral assemblage, some minerals precipitate and redissolve as reaction progress increases. Two minerals that precipitate and redissolve in the reaction-progress range 10^{-2} to 10^{-1} and are not shown in Fig. 7 because of crowding are calcite ($<4 \times 10^{-4}$ moles/kg water) and dolomite ($<3 \times 10^{-5}$ moles/kg water). At 25°C, the final mineral assemblage contains quartz, kaolinite, sodic muscovite, nontronite, paragonite, calcite, and saponite; hematite and dolomite precipitate and redissolve during the calculation. At 125°C, the final mineral assemblage contains quartz, beidellite, saponite,

nontronite, plagioclase, and sodic muscovite; hematite, calcite, and prehnite precipitate and redissolve during the calculation. None of the zeolites observed at Yucca Mountain are part of the mineral assemblages for this case.

Doubling or halving the Al^{3+} dissolution rate had little effect on the results at 75°C. Solution pH and total dissolved silica content remain about the same. The identity of minerals in the final solid-phase assemblage is also generally the same. With a low Al^{3+} dissolution rate, more quartz and less clay precipitates, and plagioclase precipitates at a reaction progress of $\sim 10^{-1}$. With a high Al^{3+} dissolution rate, more clay and less quartz precipitates. Varying the Fe^{3+} dissolution rate mainly affects precipitation of nontronite, an iron-rich smectite clay. Essentially all the iron from the volcanic glass precipitates in this form. The results for the aqueous phase are essentially unaffected by changes in the Fe^{3+} dissolution rate.

None of the mineral assemblages predicted for this case contain the zeolites clinoptilolite or mordenite that have been observed at Rainier Mesa and other NTS locations. Also, the dissolved silica content of the aqueous phase is lower than observed for Rainier Mesa water except at 125°C. Because cristobalite rather than quartz is usually associated with clinoptilolite and mordenite, it may be necessary to have a higher $SiO_2(aq)$ activity to precipitate these zeolites. This question is investigated in the following section.

B. Quartz and Chalcedony Precipitation Suppressed

A number of calculations were done in which precipitation of quartz and chalcedony was suppressed to increase $SiO_2(aq)$ activity. In addition, precipitation of nontronite was suppressed in most of these calculations to control the clay precipitate composition. Figure 8 shows a plot of aqueous-phase pH for runs at 25, 75, 125, and 175°C, in which precipitation of quartz, chalcedony, and nontronite was suppressed. The final values of pH, where the system is controlled by the solid-phase assemblage, are from 7 to 8.5; the results from the 75, 125, and 175°C calculations are in the range observed at Rainier Mesa. At pH 7, the total dissolved silica content is 0.36 mmolal at 25°C, 1.32 mmolal at 75°C, 3.1 mmolal at 125°C, and 5.8 mmolal at 175°C. Thus, the 75°C result agrees best with the range observed at Rainier Mesa (0.7 to 1.3 mmolal). Higher temperature conditions could also be in agreement with observed silica content if it is assumed that some solid silica precipitation occurs as a sample is cooled to room temperature.

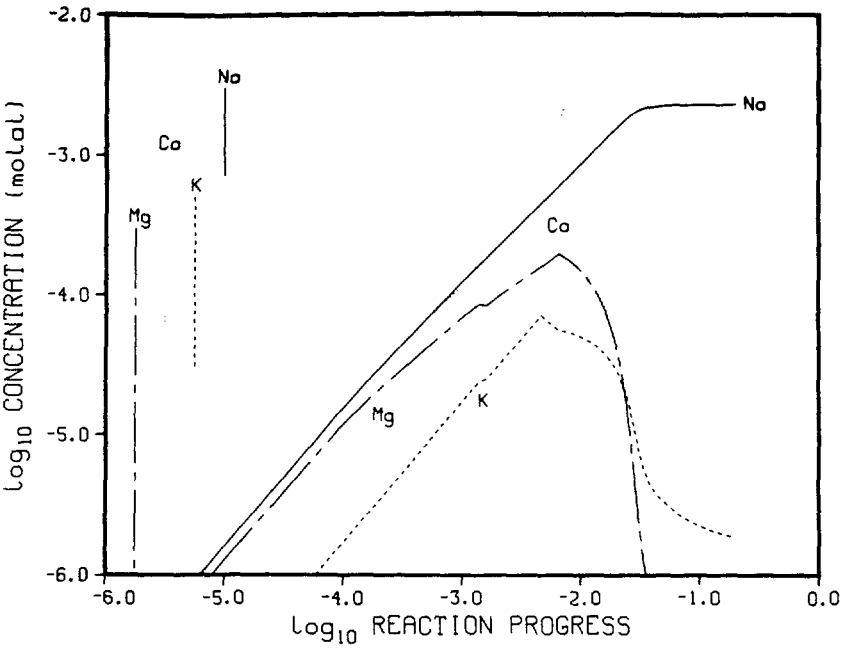

Fig. 9. Total sodium, potassium, calcium, and magnesium content of the aqueous phase at 75°C. Precipitation of quartz, chalcedony, and nontronite suppressed. Vertical lines at left show ranges observed at Rainier Mesa.

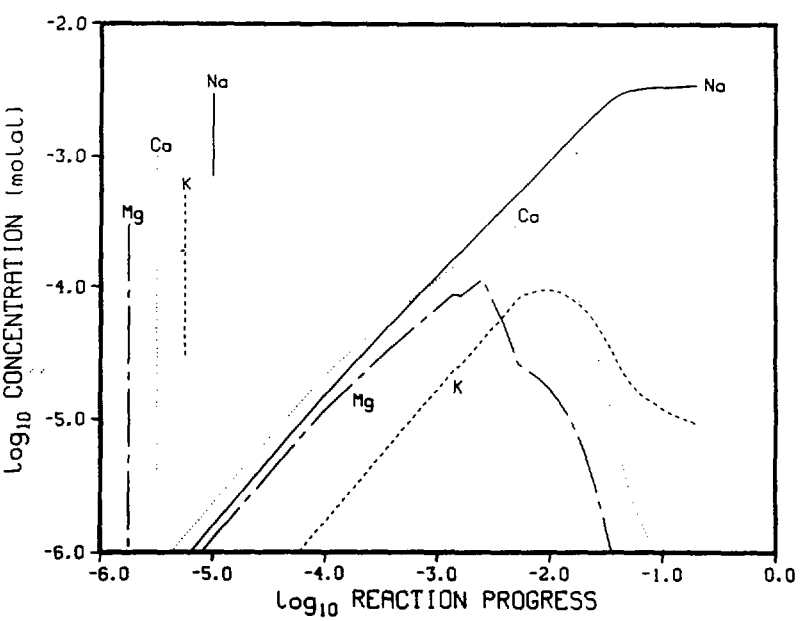

Fig. 10. Total sodium, potassium, calcium, and magnesium content of the aqueous phase at 125°C. Precipitation of quartz, chalcedony, and nontronite suppressed. Vertical lines at left show ranges observed at Rainier Mesa.

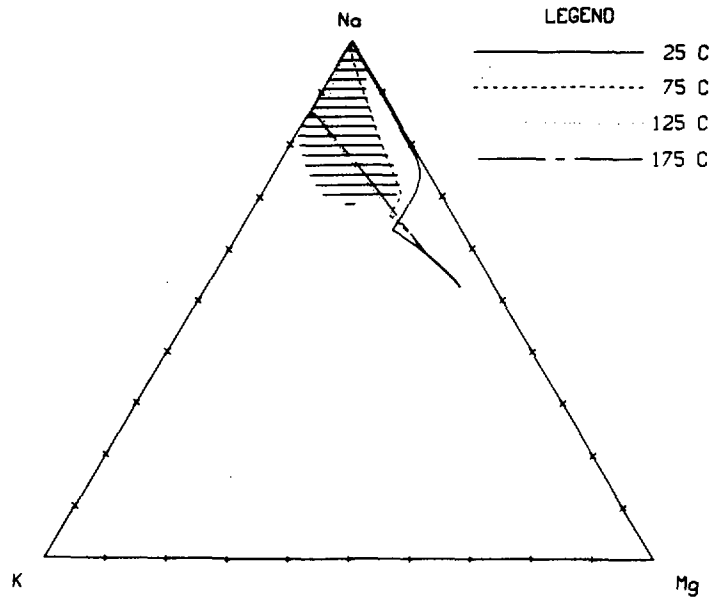

Fig. 12. Relative Na-K-Mg content of the aqueous phase. Precipitation of quartz, chalcedony, and nontronite suppressed.

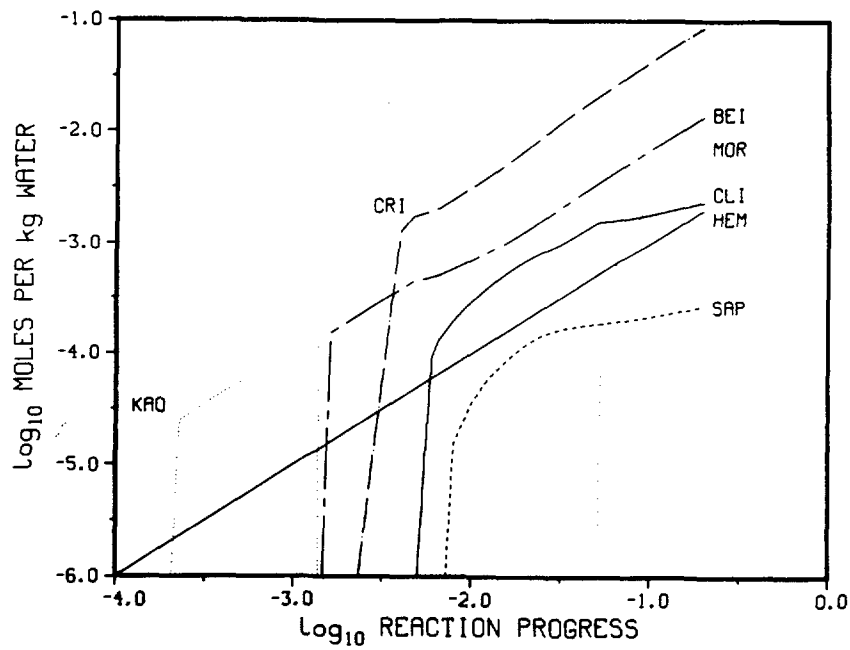

Fig. 13. Mineral precipitates at 75°C. Precipitation of quartz, chalcedony, and nontronite suppressed. Mineral abbreviations listed in Appendix.

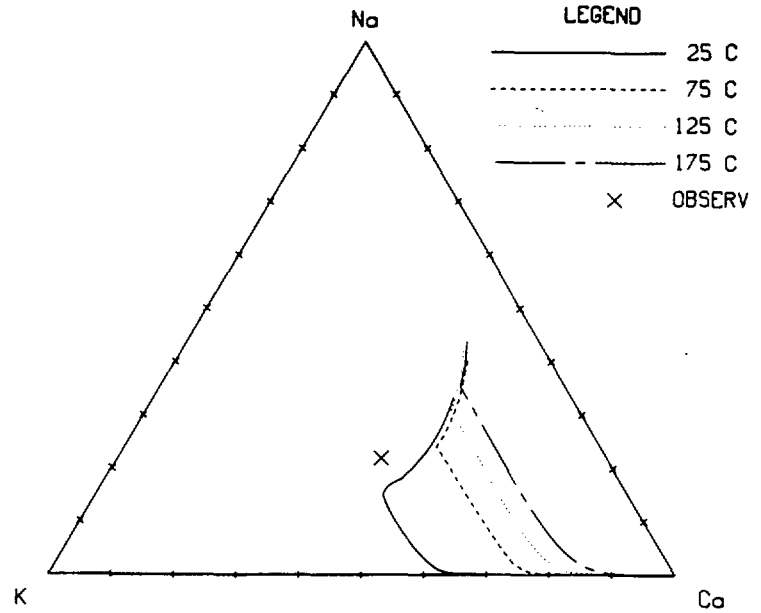

Fig. 14. Relative Na-K-Ca content of clinoptilolite precipitate. Precipitation of quartz, chalcedony, and nontronite suppressed. The x locates the average clinoptilolite composition observed at Rainier Mesa.

still precipitates initially, but it is replaced early in the reaction path by nontronite as the iron-bearing mineral. The remainder of the phase assemblage, including the presence of beidellite, is essentially the same as when nontronite precipitation is suppressed; there are small changes in the quantities of other minerals and compositions of other solid solutions to account for the presence of nontronite. Thus, the reaction-path calculations indicate that iron will precipitate in smectite clays or, if the kinetics of clay precipitation are too slow, as hematite.

Doubling the Al^{3+} dissolution rate in the case where precipitation of quartz and chalcedony is suppressed has little effect on the aqueous-phase results at 75°C. In the final solid-phase assemblage, the quantities of cristobalite and clinoptilolite were reduced, whereas the quantity of beidellite was increased. Saponite precipitated initially at about the same value of reaction progress, but it redissolved before the end of the calculation. Reducing the Al^{3+} dissolution rate by half at 75°C also has little effect on the aqueous-phase results. The minerals precipitated are the same as those with the nominal Al^{3+} dissolution rate; the quantities of cristobalite and clinoptilolite are increased and the quantity of beidellite

In this case, reducing the relative Al^{3+} dissolution rate from the glass to half its nominal value has a significant effect. At 75°C, amorphous silica now precipitates, and talc replaces pyrophyllite and beidellite as clay precipitates. The zeolites clinoptilolite and mordenite are also in the stable mineral assemblage. The pH of the aqueous phase increases to 7.2, which is within the observed range for Rainier Mesa water. However, the total dissolved silica content of the aqueous phase is still quite high (4.6 mmolal), and the magnesium content of the aqueous phase is also high. Doubling the Al^{3+} dissolution rate for this case merely leads to more clay precipitates with essentially no other effects. Increasing or decreasing the Fe^{3+} dissolution rate modifies the amount of hematite or nontronite precipitate in a like manner but has few other effects.

Agreement between calculated and observed water compositions and mineral assemblages is not as good in this case as in the previous one, where only quartz and chalcedony precipitation was suppressed. By reducing the Al^{3+} dissolution rate, agreement was improved somewhat; however, the total dissolved silica and magnesium contents of the aqueous phase are still too high.

D. Precipitation of Albite and Analcime

Results from calculations discussed in the previous sections have shown the formation of cristobalite, smectite clays, and the zeolites clinoptilolite and mordenite from dissolution of volcanic glass by using a simple reaction-path model. However, this is only the first stage in the mineral evolution scheme that has been proposed for NTS (Hoover 1968; Moncure et al. 1981; Waters and Carroll 1981). Further evolution leads to mineral assemblages that contain analcime and then albite. The steps in this sequence have been related to zones of increasing temperature (Iijima 1978). However, the reaction-path calculations in which precipitation of quartz and chalcedony was suppressed indicated that the same cristobalite, smectite, and zeolite mixture was stable up to 175°C, well above the temperature at which further steps in the sequence have been seen in field observations. The fact that $SiO_2(aq)$ activity had to be maintained higher than quartz equilibrium to achieve this mineral assemblage indicates that $SiO_2(aq)$ activity may be a controlling variable. This does not contradict observations pointing to temperature because increasing temperature may be related to faster quartz precipitation kinetics and a decrease in $SiO_2(aq)$ activity. In fact, the total dissolved silica

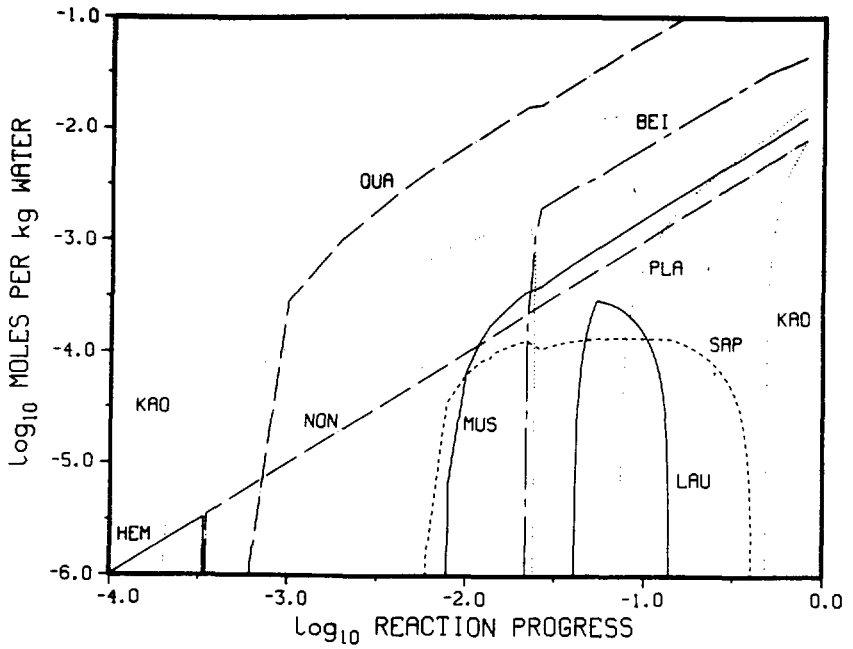

Fig. 15. Mineral precipitates at 75°C. Precipitation of paragonite and sodic muscovite suppressed. Mineral abbreviations listed in Appendix.

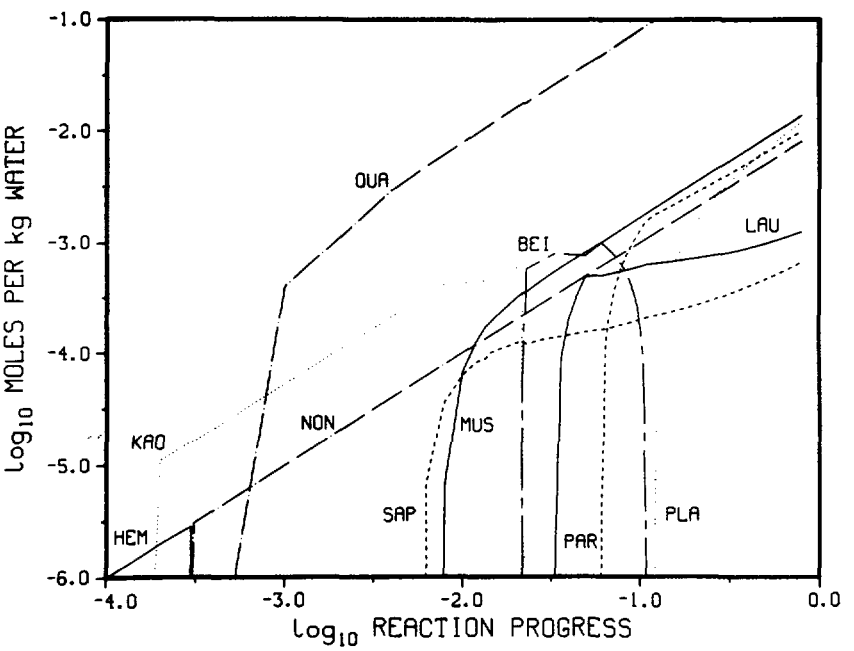

Fig. 16. Mineral precipitates at 75°C. No mineral precipitates suppressed. Al^{3+} dissolution rate from glass half the nominal value. Mineral abbreviations listed in Appendix.

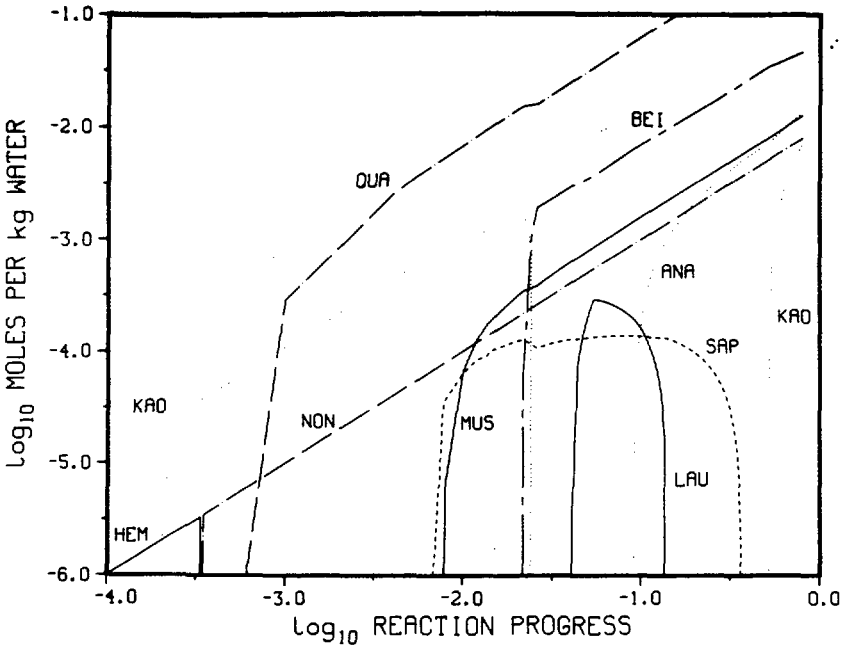

Fig. 17. Mineral precipitates at 75°C. Precipitation of paragonite, sodic muscovite, and all albite minerals suppressed. Mineral abbreviations listed in Appendix.

assumed in the calculations. At several kilobars pressure, the activity of water increases enough to drive the reaction to the left, making analcime stable with respect to albite at low temperatures (Helgeson et al. 1978). The relative stability of albite and analcime may thus be a function of total pressure, which was not considered as a variable here because of present limitations in EQ3/6.

E. Dissolution Rates Proportional to Relative Composition

So far, all the reaction-path calculations have used volcanic-glass dissolution rates based on the measurements of White et al. (1980) and assumed rates for Al^{3+} and Fe^{3+}. If dissolution-rate measurements had not been made, congruent dissolution would have been a logical assumption to use for these calculations. A reaction-path calculation was done at 75°C by using dissolution rates that are proportional to the relative composition of the glass (White et al. 1980) to see the effect this would have on the results. Table IV compares the dissolution rates based on composition with rates used previously at pH 5 and 7. The major differences occur with K^+, Ca^{2+}, and Mg^{2+}. Based on composition, K^+ has a much higher dissolution rate, and Ca^{2+} and Mg^{2+} have much lower rates than measurements indicate.

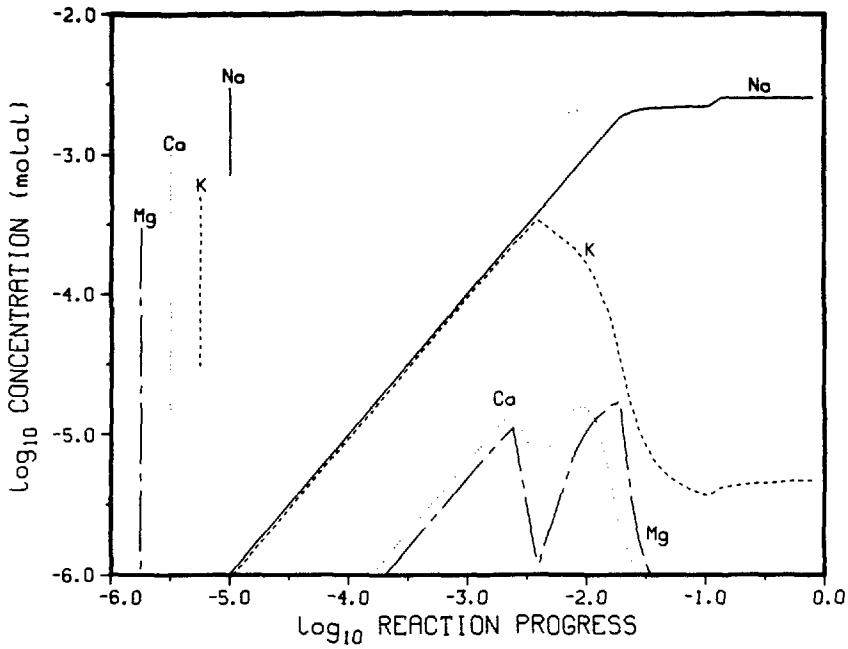

Fig. 18. Total sodium, potassium, calcium, and magnesium content of the aqueous phase. Precipitation of quartz, chalcedony, and nontronite suppressed. Congruent dissolution of volcanic glass.

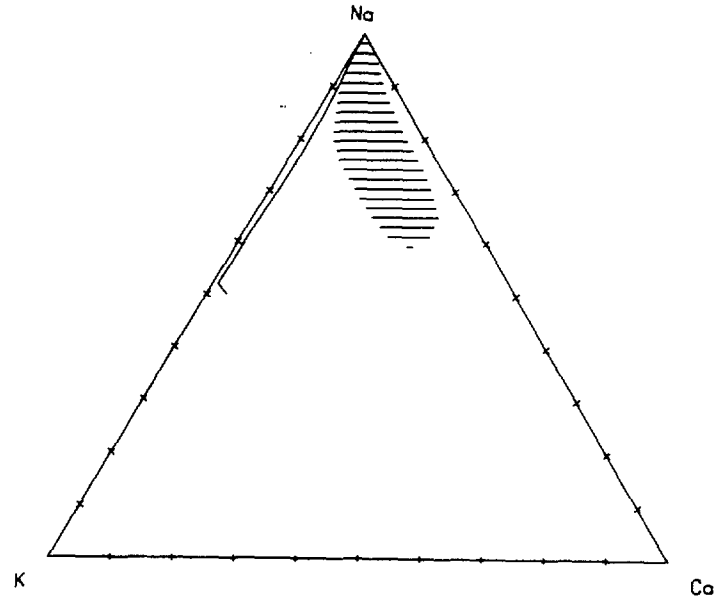

Fig. 19. Relative Na-K-Ca content of the aqueous phase. Precipitation of quartz, chalcedony, and nontronite suppressed. Congruent dissolution of volcanic glass.

V. SUMMARY AND DISCUSSION

This paper describes a reaction-path calculation of groundwater chemistry and mineral formation at Rainier Mesa. The calculation is based on a model proposed by Claassen and White (1978) in which water saturated with CO_2 reacts with volcanic glass. The various species composing the glass are leached or dissolved at different rates. Measured dissolution rates for $SiO_2(aq)$, Na^+, K^+, Ca^{2+}, and Mg^{2+} from Rainier Mesa glass were used; rates for Al^{3+} and Fe^{3+} were assumed. Groundwater chemistry is related to the relative dissolution rates of species from the glass and the minerals that precipitate during the dissolution process. The reaction-path calculation models this irreversible process as a sequence of equilibrium states in which relative dissolution rates control the total amounts of various species available; equilibrium thermodynamics is used to partition each species among the aqueous phase and possible mineral phases. Minerals that precipitate during the calculation remain in contact with the aqueous phase and can redissolve if conditions are appropriate. Precipitation of certain minerals was suppressed during some calculations to control aqueous-phase activities.

The EQ3/6 chemical equilibrium computer programs were used for these calculations. Although the thermodynamic data base for these programs is extensive, data for three zeolites found at NTS (clinoptilolite, heulandite, and mordenite) were not available. These data were estimated from 0 to 300°C by using the method proposed by Chen and thermodynamic data from the EQ3/6 data base.

The primary purpose of this work was to test whether equilibrium processes could be used to explain groundwater chemistry and minerals found at Rainier Mesa, Yucca Mountain, and other NTS locations. A number of qualitative discussions of zeolite formation have proposed the same general model, interaction of groundwater with volcanic glass, for this process (Hoover 1968; Moncure et al. 1981). Claassen and White (1978) made this model more quantitative by proposing a specific starting point and by measuring important rate processes involved in glass dissolution. This work makes the model still more quantitative by requiring that a reaction-path calculation be used to predict water composition and mineral precipitates. Although rate processes may control the availability of species through the dissolution process, the reaction-path calculation imposes equilibrium constraints at each step in the path and thus leaves little to the choice of the modeler. Of course, it is

The next stages of mineral evolution involve a quartz, analcime, and illite mixture followed by a quartz, albite, and potassium-feldspar mixture. The stages in this sequence have been related to zones of increasing temperature (Iijima 1978); however, reaction-path calculations done here indicate that higher temperatures alone do not change the mineral assemblage from cristobalite, zeolite, and smectite clay as long as the SiO_2(aq) activity remains high. Mineral assemblages that would result from lower SiO_2(aq) activities were determined from reaction-path calculations in which quartz was allowed to precipitate. The results show that albite is part of the mineral assemblage in that case and that analcime precipitates if albite precipitation is suppressed. Quartz, smectite clays, kaolinite, mica, and the zeolite laumontite are also part of the mineral assemblages, depending on the exact conditions (see Figs. 15 through 17). There are some areas of disagreement between calculated results and observations for this case. In particular, the aqueous-phase pH rises above the 7 to 8 range observed for Rainier Mesa water whenever the SiO_2(aq) activity is reduced to a level in equilibrium with quartz, although at 125°C the difference is small (see Fig. 4). Also, the relative potassium content tends to be low (see Fig. 6). Finally, the mineral assemblages, particularly the formation of analcime and then albite, do not occur as expected without additional constraints. Overall, the agreement between calculations and observations for this case is fair.

The reaction-path calculations discussed here can be interpreted to give an overall scheme for mineral formation at Rainier Mesa and similar NTS locations. Volcanic glass dissolution rates and slow quartz precipitation kinetics combine to give conditions necessary for precipitation of cristobalite, zeolites, and smectite clays. Because the SiO_2(aq) activity is high, zeolites such as clinoptilolite and mordenite, which have high silicon/aluminum ratios, are favored. Over longer periods of time or with increasing temperature, SiO_2(aq) activities are reduced to levels in equilibrium with quartz. Clinoptilolite and mordenite are no longer stable. Whether analcime or albite forms may depend on precipitation kinetics or may be an equilibrium process that is a function of temperature. The thermodynamic data used here indicate that kinetics must be involved if analcime precipitates, but other thermodynamic data allow equilibrium processes only. The importance of the relative dissolution rates of the volcanic glass is evident from the calculation in which congruent dissolution was assumed. The effects of glass dissolution

REFERENCES

F. Caporuscio, D. Vaniman, D. Bish, D. Broxton, B. Arney, G. Heiken, F. Byers, R. Gooley, and E. Semarge (1982) "Petrologic studies of drill cores USW-G2 and UE25b-1H, Yucca Mountain, Nevada," Los Alamos National Laboratory report LA-9255-MS.

C. Chen (1975) "A method of estimation of standard free energies of formation of silicate minerals at 298.15 K," Am. J. Sci. 275, 801-817.

H. C. Claassen and A. F. White (1978) "Application of geochemical kinetic data to groundwater systems, a tuffaceous-rock system in Southern Nevada," in Chemical Modeling in Aqueous Systems, E. A. Jenne, Ed., Amer. Chem. Soc. Symposium Series 93, 771-793.

W. D. Dibble, Jr., and W. A. Tiller (1981) "Kinetic model of zeolite paragenesis in tuffaceous sediments," Clays Clay Miner. 29, 323-330.

E. H. Essington and J. V. Sharp (1968) "Some aspects of groundwater solution chemistry, underground nuclear explosion zones, Nevada Test Site," in Nevada Test Site, E. B. Eckel, Ed., Geol. Soc. Am. Mem. 110, 263-273.

H. C. Helgeson (1968) "Evaluation of irreversible reactions in geochemical processes involving minerals and aqueous solutions - I. Thermodynamic Relations," Geochim. Cosmochim. Acta 32, 853-877.

H. C. Helgeson, R. M. Garrels, and F. T. Mackenzie (1969) "Evaluation of irreversible reactions in geochemical processes involving minerals and aqueous solutions - II. Applications," Geochim. Cosmochim. Acta 33, 455-481.

H. C. Helgeson, T. H. Brown, A. Nigrini, and T. A. Jones (1970) "Calculation of mass transfer processes involving aqueous solutions," Geochim. Cosmochim. Acta 34, 569-592.

H. C. Helgeson, J. M. Delany, H. W. Nesbitt, and D. K. Bird (1978) "Summary and critique of the thermodynamic properties of rock-forming minerals," Am. J. Sci. 278A, 1-229.

J. D. Hem (1970) "Study and interpretation of the chemical characteristics of natural water," US Geol. Survey Water-Supply Paper 1473 (2nd ed.).

D. L. Hoover (1968) "Genesis of zeolites, Nevada Test Site," in Nevada Test Site, E. B. Eckel, Ed., Geol. Soc. Am. Mem. 110, 275-283.

A. Iijima (1978) "Geologic occurrences of zeolites in marine environments," in Natural Zeolites: Occurrence, Properties, Use, L. B. Sand and F. A. Mumpton, Eds. (Pergamon Press), pp. 175-198.

T. E. C. Keith, D. E. White, and M. H. Beeson (1978) "Hydrothermal alteration and self-sealing in Y-7 and Y-8 drill holes in northern part of Upper Geyser Basin, Yellowstone National Park, Wyoming," US Geol. Survey Professional Paper 1054-A.

T. J. Wolery (1979) "Calculation of chemical equilibrium between aqueous solution and minerals: The EQ3/6 software package," Lawrence Livermore Laboratory report UCRL-52658.

T. J. Wolery (1980) "Chemical modeling of geologic disposal of nuclear waste: Progress report and a perspective," Lawrence Livermore Laboratory report UCRL-52748.

Solid Solutions

Beidellite (BEI)

$X_{0.33}[Al_{2.33}Si_{3.67}O_{10}](OH)_2$, X = H, Na, and K

$Y_{0.165}[Al_{2.33}Si_{3.67}O_{10}](OH)_2$, Y = Ca and Mg

Clinoptilolite (CLI)

$X_2[Al_2Si_{10}O_{24}]\cdot 8H_2O$, X = Na and K

$Y[Al_2Si_{10}O_{24}]\cdot 8H_2O$, Y = Ca and Mg

Mordenite (MOR)

$X[AlSi_5O_{12}]\cdot 3H_2O$, X = Na and K

Nontronite (NON)

$X_{0.33}[Al_{0.33}Si_{3.67}Fe_2O_{10}](OH)_2$, X = H, Na, and K

$Y_{0.165}[Al_{0.33}Si_{3.67}Fe_2O_{10}](OH)_2$, Y = Ca and Mg

Plagioclase (PLA)

Low albite - $NaAlSi_3O_8$

Anorthite - $CaAl_2Si_2O_8$

Saponite (SAP)

$X_{0.33}[Al_{0.33}Si_{3.67}Mg_3O_{10}](OH)_2$, X = H, Na, and K

$Y_{0.165}[Al_{0.33}Si_{3.67}Mg_3O_{10}](OH)_2$, Y = Ca and Mg

Sodic muscovite (SOD)

Paragonite - $NaAl_3Si_3O_{10}(OH)_2$

Muscovite - $KAl_3Si_3O_{10}(OH)_2$

★U.S. GOVERNMENT PRINTING OFFICE: 1983-0-776-026/120

Printed in the United States of America
Available from
National Technical Information Service
US Department of Commerce
5285 Port Royal Road
Springfield, VA 22161

Microfiche (A01)

Page Range	NTIS Price Code	Page Range	NTIS Price Code	Page Range	NTIS Price Code	Page Range	NTIS Price Code
001-025	A02	151-175	A08	301-325	A14	451-475	A20
026-050	A03	176-200	A09	326-350	A15	476-500	A21
051-075	A04	201-225	A10	351-375	A16	501-525	A22
076-100	A05	226-250	A11	376-400	A17	526-550	A23
101-125	A06	251-275	A12	401-425	A18	551-575	A24
126-150	A07	276-300	A13	426-450	A19	576-600	A25
						601-up*	A99

*Contact NTIS for a price quote.